Journal of Materials Chemistry B

PAPER

View Article Online
View Journal | View Issue

Cite this: J. Mater. Chem. B, 2014, 2, 981

Magnetic, optical gold nanorods for recyclable photothermal ablation of bacteria†

Mohankandhasamy Ramasamy,[a] Su Seong Lee,[b] Dong Kee Yi*[c] and Kwangmeyung Kim*[d]

Received 21st September 2013
Accepted 20th November 2013

DOI: 10.1039/c3tb21310b

www.rsc.org/MaterialsB

A new antibacterial gold nanorod (GNR) conjugated magnetic nanoparticle (MNP) composite (GNR–MNP) was synthesized successfully for the eradication of antibiotic resistant nosocomial pathogens in water to improve the water quality. The composite was fabricated *via* the reaction of nucleophilic amine and epoxide carbon moieties with silanes. Tagging of MNP over GNR was confirmed using electron microscopy. Zeta potential measurements were used to study the fundamental surface chemical states of GNR and MNP (before and after surface modification). The synthesized GNR–MNP composite was directly mixed with a bacterial culture suspension and the photo-thermally induced bactericidal effects were evaluated before and after laser treatment. Optical, spectral and electron microscopy results revealed that laser irradiated GNR–MNP show a more pronounced bactericidal effect than other disinfecting agents. Further, the results indicate that there is a positive correlation between the bacterial cell mortality and nanoparticle concentration and laser energy used. Interestingly, GNR–MNPs are capable of generating a rapid and reiterated photothermal effect for more than three consecutive cycles with enhanced magnetic separation for repeatable bactericidal application. These results suggest that the fabricated GNR–MNPs are a highly efficient photothermal agent against a wide variety of bacteria, suitable for cleaning real samples like water. Importantly, our method showed superior cell lysing results for both *Escherichia coli* (*E. coli*) and *Enterococcus faecalis* (*E. faecalis*) compared to conventional heat treatment.

Introduction

In recent years noble metals, especially anisotropic gold, have fascinated researchers with their unique optical, electronic, shape dependent chemical and photophysical properties.[1] Different derivatives of nanogold materials have been developed with various applications in imaging, sensing, and as drug or DNA delivery vehicles.[2–8] In addition, the gold crystal lattice can convert absorbed optical energy into homogeneous heat energy, which is transferred to the surrounding media *via* phonon–phonon relaxation, making gold a promising agent for photothermal therapy.[9–13] Gold nanoparticles in combination with laser energy have been used to detect and destroy various cancer cells, viruses and bacteria.[14–16] Due to their dimension dependent properties, gold nanorods show enhanced opto-thermal efficiency due to their large absorption surface area compared to other forms of nanogold.

Emerging drug resistance in microbes has motivated researchers to work with new advanced techniques to synthesis highly efficient anti-microbial agents. Compared to the bulk phase, nanoscale metals exhibit potent microbicidal, bactericidal, fungicidal and viricidal properties due to their greater surface area and better contact efficiency.[17] As an alternative to conventional methods, the photothermal phenomenon can be utilized to lyse bacteria by rapidly generated heat using GNRs and laser light which increases the temperature of the surrounding media with low thermal conductivity.[1,18–20] This elevated temperature has been shown to cause a significant reduction in bacterial survival rates,[21] suggesting that photo-induced heating may be an alternative method for bacteria lysis, based on rupturing membranes.

Hybridisation, the magnetic properties and NIR photo-heating, in each nanocomposite provides a platform for simultaneous bio-labeling, cell separation and photothermal applications.[22,23] Electrostatic attachment of iron nanoparticles on polymer coated GNRs has been carried out for better magnetic manipulation.[24] Thiol-functionalized, gold coated, iron nanoparticles have been used for detection and bio-separation of bacteria.[25] The reported nanoparticles suffered from either aggregation after coating or nanoparticle melting during NIR laser irradiation,[26,27] preventing re-use. However,

[a]Department of Bionanotechnology, Gachon University, Seongnam, 461701, Korea
[b]Institute of Bioengineering and Nanotechnology, The Nanos, Singapore, 138669
[c]Department of Chemistry, Myongji University, Yongin, 449-728, Korea. E-mail: vitalis@mju.ac.kr; kim@kist.re.kr
[d]KIST, Center for Theragnosis, Biomedical Research Institute, Seoul, 136791, Korea

† Electronic supplementary information (ESI) available. See DOI: 10.1039/c3tb21310b

coating GNRs with silica and combining this with MNPs could alter the aforementioned disadvantages, due to the protective surface covering and incorpoated magnetic property.

In this study we propose new coating technologies for unique nucleophilic hybridization of two different nanomaterials producing a reusable anti-microbial agent. The mortality rate of both types of bacteria was measured in two scenarios: photothermal therapy and the heating method. It was demonstrated that photoheating with a laser in the presence of GNRs can destroy the living cells.[13–15] Hence in this work we have utilized GNR–MNPs with laser light to elucidate their bactericidal properties. Further, we assessed the repeated bacteria lysis of a single solution of GNR–MNPs and compared the rate of bacteria destruction to that observed with the conventional method.

Synthetic methods

Bacterial culture

The *Escherichia coli* (*E. coli* KACC 10005), and *Enterococcus faecalis* (*E. faecalis* KACC 13807), were cultured in Luria–Bertani broth (LB broth, Miller, AMERSCO, USA) to a concentration of 10^8 colony forming units per ml (CFU ml^{-1}).

Preparation and characterization of GNR–MNPs

Step I: preparation and surface modification of GNRs. GNRs were prepared based on the method outlined in previous reports.[28,29] A thin silica coating on GNR was formed using 10 mM 3-mercaptopropyl trimethoxysilane (MPTMS, Sigma-Aldrich, USA) for 12 h under stirring. Then ammonium hydroxide at pH 9 was added with continuous stirring. Silica coated GNRs were washed three times with ethanol before proceeding the next step.

Step II: synthesis of epoxide GNRs (epo-GNRs). Silica coated GNRs were first reacted with 10 μl of *N*-ethyldiisopropylamine (*N*-EDIPA, Alfa Aaesar) then with 5 μl of 5,6-epoxyhexyltriethoxysilane (ETES, Gelest Inc. USA) in the presence of 100 μl de-ionized water and shaken overnight at room temperature. Unbound particles were removed by washing with ethanol.

Step III: surface modification of MNPs and conjugation with epo-GNRs. By using tetraethylorthosilicate (TEOS, Sigma-Aldrich, USA), the silica coated MNPs were synthesized as described in detail in the literature.[30] For a typical amine immobilization, clean silica coated particles were dispersed in absolute ethanol. Next, 90 μl ammonium hydroxide was added to the dispersion and the pH was adjusted to 9. Subsequently, 30 μl of 3-aminopropyltrimethoxysilane (3-APTMS, Sigma-Aldrich, USA) solution in ethanol was added drop-wise under continuous stirring for 16 h.

To synthesize GNR–MNPs, 2 ml of previously modified GNRs was added to 0.1 ml surface modified MNP in the presence of 2 μl *N*-EDIPA, and the mixture was shaken overnight. Conjugated particles were washed and collected by centrifugation in ethanol. The purified samples were re-dispersed in de-ionized water from ethanol for further characterization.

Characterization

The absorbance spectra of the GNRs were recorded in the UV–Visible–NIR region using a Varian CARY 50 (Varian Inc.) spectrophotometer with a quartz cell. Zeta-potential measurements of the nanoparticles were taken using a Malvern Zeta-Sizer 3000HS instrument. Morphology and elemental analysis were studied using a high-resolution transmission electron microscopy interfaced with energy dispersive X-ray spectroscopy (HR-TEM-EDX, Tecnai G2 TF 30ST).

Photothermal efficiency of GNR–MNPs

The GNR–MNPs were placed in a microcentrifuge tube and the bottom was covered with inverted aluminum foil to prevent strewing of the laser beam and as a reflexive aid. A red light from the DPSS laser (Dream laser system, Japan) with a central wavelength of 671 nm was used as the excitation source and the temperature difference was recorded with a thermocouple (K type, Omega) interfaced with a data acquisition system (34970, Aglient, CA, USA).

Optimization of nanoparticle concentration

Initially, to fix the optimum quantity of GNR–MNPs which was most suitable for all the experiments, different concentrations of the sample, including 5, 10, 15, 20, 25, 30 and 35 mg ml^{-1} were tested. The GNR–MNPs were irradiated continuously to attain an unchanged maximum temperature at the fixed laser power (130 mW). Each experiment was repeated three times and the acquired values were used to plot a temperature–time dependant curve (*T*–*t* curve).

Photothermal repeatability

The efficiency of the nanoparticles was examined to establish the repeatablity of the photothermal heating property for attaining a single desired temperature. The GNR–MNPs were irradiated to attain an unchanged maximum temperature; under exposure to light over an extended time period. This process was repeated until there was a complete reduction in the elevated temperature, corresponding with time. Variation in the nanoparticle mass, before and after laser exposure, was monitored using the dry weight method.

Photothermal evaluation of bacteria viability

Aliquots of microbial suspensions containing GNR–MNPs were irradiated in the tube. The resulting suspension was added to saline and re-dispersed by vigorous vortexing. An external magnet was bound and the supernatant was gently removed with a pipette. The magnetically collected nanoparticles were further suspended with fresh bacteria for repeated measurement of the photothermal activity. In addition, the removed bacteria suspension was stained using a Live/Dead® BacLight™ Bacterial Viability Kit (Invitrogen) as per the manufacturer's protocol. The stained sample was covered with glycerin and a cover glass and examined using laser scanning fluorescence microscopy (Nikon Eclipse TE 2000-U). Individual cells were

quantified by counting randomly at least five fields of view and a minimum of 200 cells per slide in triplicate.

In addition, to corroborate the photothermal impact, the change in surface morphology of the bacteria before and after laser irradiation was observed using the field emission scanning electron microscopy interfaced with energy dispersive X-ray spectroscopy (FE-SEM-EDX; JEOL-JSM-7500F, Tokyo, Japan).

Meanwhile, detailed elemental analysis was performed for the GNR–MNPs after every photothermal cycle. The magnetically separated GNR–MNPs were washed twice with de-ionized water and examined under the FE-SEM interfaced EDX analyzer after each cycle and the results were plotted. The same concentration of nanoparticles without bacteria was used as a control.

Laser power efficiency

Further, a comparative study of bactericidal quantification with increasing laser power output was analyzed. The bacterial suspensions were mixed with GNR–MNPs (20 mg ml^{-1}), and irradiated by a laser with varying power densities of 10, 30, 60, 90 and 130 mW. Each time the treated suspension was separated and examined under a microscope.

Proliferation assay

A fluorescence spectrophotometer (Varian, Cary Eclipse spectrofluorometer) was adopted to determine the difference in fluorescence intensity produced by the laser treated, dye added bacterial samples with an excitation range between 450 nm and 490 nm and detected emissions at around 520 nm and 630 nm for green (live) and red (dead) fluorescence, respectively.

Biocidal activity of GNR–MNPs

Bacterial suspensions with approximately 10^8 CFU ml^{-1} were prepared separately for each culture with an initial optical density (OD_{600}) of 0.1. Typically, 20 mg ml^{-1} of GNR–MNPs were added to the bacterial suspension. After laser irradiation, the suspension was vortexed, and the GNR–MNPs were separated from the bacteria using an external magnet. Then the difference in absorbance caused by dead cells was monitored with UV–Visible spectrophotometer.

Influence of direct heat

Initially, the difference between the photo-thermally induced heat and the heat bath mounted on hot-plate (Heidolph, MR Hei standard, 850 W) produced heat was compared and their corresponding thermal responses with time were plotted.

Later, to analyze the impact of direct heat on viability, the bacterial suspensions were incubated in a hot-plate enabled heat bath at different temperature intervals ranging from 40 °C to 100 °C. Heat treated bacterial suspensions were left to cool at room temperature and were mixed with the dye to examine the dead cells by fluorescence microscopy.

Statistical analysis

Triplicate experiments were carried for each sample and the results were expressed as mean ± standard deviation (SD). A one-way analysis of variance (ANOVA) was used for data analysis. A "p" value of ≤ 0.05 was considered to be statistically significant.

Results and discussion

Preparation and characterization of GNR–MNPs

GNRs were constructed in aqueous solution using a cationic surfactant directed seed-mediated method.[31] Both the GNR and MNP were surface modified and GNR–MNPs were formed by nucleophilic conjugation.

The zeta potential values of the silica coated GNRs and MNPs were −28 mV and −30.6 mV, respectively. Upon further deposition of 3-APTMS (for MNP) and 5,6-ETES (for GNR), the zeta potential charges reversed to +21.4 mV and +25.3 mV, confirming the deposition of cationic groups on the surface of the nanomaterials.

Fig. 1a, b and d show HR-TEM images of the GNR–MNPs. Easily distinguishable layers of surface coating on the nanoparticles were clearly visible from the images. Furthermore, the EDX shows the combination of Au, Fe and Si in the GNR–MNPs, along with C, O and Cu, which confirms successful conjugation between the two different nanomaterials upon surface modification.

The UV–Vis–NIR spectrum of the GNRs was characterized by a small peak at 520 nm and an intense plasmon resonance peak at 650 nm. In addition, the GNRs experienced alterations to their optical properties before and after surface modification (Fig. 1e). Bathochromic shifts of 6 and 16 nm in the longitudinal peak are observed for silica coated GNRs and epo-GNRs respectively. The small shift confirms a thin coating of silica, whereas a large shift in the absorbance spectrum indicates that the epoxide group bearing ETES was successfully coated on the GNRs.

Prior to conjugation, CTAB free GNRs were treated with MPTMS, the –SH groups were attached to the surface, and $-Si(OH)_3$ groups formed a thin silica layer on the GNRs. Subsequent post synthetic modification was accessed by applying ETES to form another layer with epoxide groups on the exterior surface. *N*-EDIPA in the presence of water acted as an auxiliary base for the reaction. The magnetic nanoparticles were silica coated by hydrolysis and subsequent condensation of TEOS in the presence of ammonium hydroxide. 3-APTMS was used as a post synthetic silanization agent leaving the amine groups at the end of nanoparticle. Epoxide-functionalized GNRs were hybridized *via* a nucleophilic reaction with the amine functionalised MNPs. The ring at the electrophilic epoxide carbon is opened to facilitate successful conjugation.[32,33] Until now, few studies have been conducted to test the direct impact of the GNR–MNP induced photothermal effect on bacteria.[22,23] Here, for the first time, we propose a new nucleophilic hybridization technique to form nanocomposites for repeated photothermal lysis of bacteria.

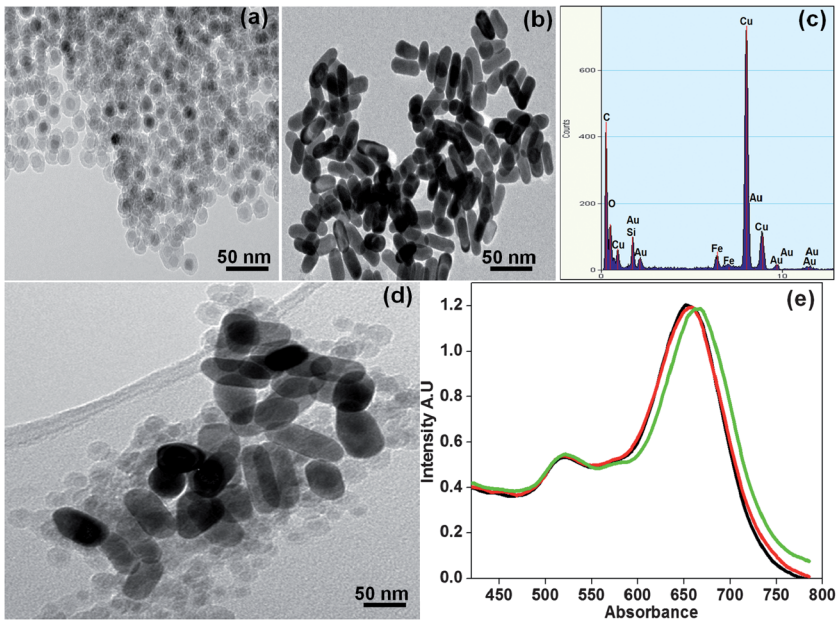

Fig. 1 HR-TEM micrographs of (a) silica coated MNPs and (b) epo-GNRs, (c) EDS spectra of conjugated nanoparticles, (d) HR-TEM micrograph of GNR–MNPs, and (e) UV–Vis spectrum of uncoated GNRs (black), silica coated GNRs (red), and epo-GNRs (green).

GNR–MNPs for photothermal lysis

The purpose of this study is to demonstrate the effect of GNR–MNPs on bacteria lysis by quickly transmitting heat through a bacterial suspension. Especially, GNRs have much larger absorption and scattering cross sections than other forms of nanoparticles which radiate heat after absorbing light. So, GNRs could be used as excellent photothermal agents for destroying pathogens.[34,35] When light strikes the GNR surface, the absorbed photon energy is transformed to a hot electron distribution by non-radiative processes in the lattice of the particle.[36] The heat effect is due to the surface plasmonic resonance of GNRs, where the gold crystal lattice is heated *via* electron–phonon interactions and is cooled by transmitting its heat to the surrounding medium *via* phonon–phonon relaxation on a picosecond time scale.[9,20] The maximum absorption of nanorods can shift to a near-infrared range which allows the light energy to be transduced into more heat energy which causes damage to the cell membranes, protein denaturation and heat stress.

The GNR–MNP concentration was optimized for effective photothermal therapy. Different concentrations were irradiated and their time to temperature response was measured. The results are illustrated in Fig. 2a as a *T*–*t* curve. The plasmonic photothermal heat dissipation pattern was measured on the basis of the method explained by An *et al.*[37] For 5, 10 and 15 mg ml^{-1} of the samples, the attained maximum temperatures after 15 min were 44.8, 53.2 and 61.8 °C, respectively. With the increasing concentrations, the maximum temperature also increased up to 70 °C for 20 mg ml^{-1}, 80 °C for 30 mg ml^{-1} and 100 °C for 35 mg ml^{-1}. After an immediate increase from room temperature to 45 °C within one minute, there was a steady, step-by-step rise in temperature up to the maximum level. A plateau temperature was recorded at the point when no further increase in temperature was observed. With respect to the increasing concentration, the GNR–MNPs were able to produce substantial temperatures. Most bacteria will not withstand high temperatures; we therefore decided to use 20 mg ml^{-1} as the optimum concentration for effective lysis. Previous research reported nanoparticles which produced an even, maximum temperature of 55 °C with NIR laser irradiation for 3 min, as highly photo-thermally efficient materials against bacteria, without considering the factor of toxicity.[38] However, our silica coated GNRs had previously been reported as non-toxic,[39] which strongly suggests that the bacterial lysis is caused only by the nanoparticle and laser combination rather than the toxicity of the nanoparticles.

Fig. 2b shows the repeated use of the laser exposed material. Initially, an optimum quantity of GNR–MNPs was selected and the temperature difference with respect to time was recorded. After irradiation, the temperature reached more than 45 °C within seconds and increased up to 70 °C, the maximum level, within 12 min. After 12 min, the temperature was not raised any further, even for particles exposed to the laser for long time periods (15 min). Comparatively, laser light irradiation of water causes negligible temperature change, MNP alone produced a temperature change up to 40 °C which is not enough to do irreparable cellular damage to the bacteria (data not shown). After the first laser irradiation the same material is applied to check for repeated temperature rise with the same conditions. Interestingly, one time laser exposed material could able to reproduce a similar photothermal response a further five times after magnetic collection. However, the five times exposed sample started showing a decrease in temperature on the sixth cycle. This is possibly due to early stages of shape deformation in the nanorods. The silica coating around the GNRs plays a vital role by preventing the initial deformation of GNRs after

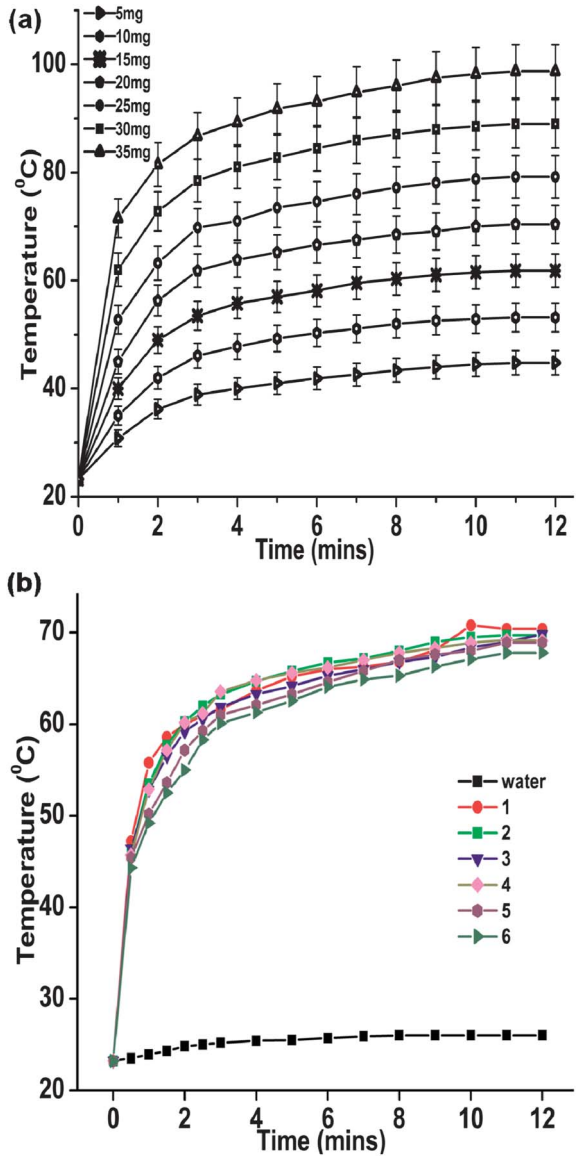

Fig. 2 (a) Temperature–time dependant curve (T–t curve) of laser irradiated GNR–MNP at different concentrations from 5 mg ml^{-1} to 35 mg ml^{-1}, (b) repeated photothermal response of a single concentration of GNR–MNPs with laser exposure.

immediate laser exposure.[40] In contrast, the uncoated GNRs do not provide reproducible temperature increase due to Ostwald ripening shape deformation on exposure to higher temperatures.[41,42] No noticeable weight losses were observed for the repeatedly laser exposed nanoparticle.

Further studies of the viability of *E. coli* and *E. faecalis* treated with GNR–MNPs were conducted using live/dead staining. The assay kit (SYTO9 and propidium iodide) was used to quantify alive and dead bacteria, from the fluorescence microscopy images. The membrane permeable dye SYTO9 enters bacteria and stains DNA to produce green color for living bacteria. Propidium iodide labeling shows dead bacteria with a red color due to the cell wall damage caused by thermolysis. Therefore, under a fluorescence microscope live bacteria with intact an cell wall are illuminated in green and dead bacteria with damaged cell walls are red (Fig. 3a). Representative bacteria viability/mortality rates are shown in Fig. 3b. The mortality rate was dramatically increased to 99% for *E. coli* and 95% for *E. faecalis* in a total of 12 min. But in the case of simple laser exposed bacteria (without nanoparticles) no significant effect on bacterial viability was observed compared to the control, thus this negligible result was similar to previous work.[43]

Fig. 3c depicts the laser power dependent bacteria mortality rate at a fixed GNR–MNP concentration. There were increasing temperatures corresponding to the increased laser densities thus causing the enhanced mortality rate. Increasing the laser power from 10 mW to 130 mW, results in a markedly higher killing rate over 12 min with respect to the corresponding temperature rises of 30 °C and 70.2 °C. More specifically, the lethal rate of bacteria at 10 mW was 5% or below. Increasing the laser intensity from 30 mW to 130 mW resulted in definite higher lysis rates from 10% to >95%, revealing the major role of laser power energy enabled photothermal impact in bacterial killing regardless of microbial type (Fig. 3a). This shows that, compared to shape specific, antibody recognizable and antibiotic release bactericidal methods,[22,44,45] exposing GNR–MNPs to laser irradiation has a strong influence on the bacterial viability, irrespective of its cell type, shape and cell wall composition. Laser exposure energy (J) = laser power (W) × exposure time (S), where J (energy) = Watt × time; therefore, it is possible to alter the penetration area by changing either the power of the lasers or the time of exposure to achieve the desired photothermal effect. Indeed, as shown, the experiments revealed the usefulness of the relationship between nanoparticle concentration, radiant energy dose and the irradiation time (Fig. 2a and 3c). The lethal laser power dependent photothermal effect of GNR–MNPs induces blebbing and vesiculation of the outer membrane, showing substantial destruction of bacteria.

Fig. 4 presents the fixed electron microscopy images of both non-irradiated and irradiated cells of *E. coli* and *E. faecalis* in live and dead conditions. It is clearly seen that the control bacteria have an intact, smooth surface with proximity in population (Fig. 4A and B). In contrast, the laser exposed bacteria exhibited significant shape modification including wrinkling, rupture with disordered of the population (Fig. 4A′ and B′). Furthermore, the magnified images, Fig. 4A″ and B″, show the cell debris, clearly representing serious damage to the bacterial walls resulted in loss of cellular components. The photothermal phenomenon of GNRs in the presence of laser light could be the key reason for the complete thermal destruction of bacteria, but as yet the clear mechanisms are not understood.

The detailed elemental analysis is shown in Fig. ES1b, (ESI).† It depicts the quantity of elements like Au, Fe, and Si in the irradiated/bacteria separated sample compared to the control. On the sixth time, there was an observable, small, reduction in the element content. Taking into account each element, compared with the control, the Au showed a nominal decrease as compared to a very minimal change in Fe, and almost no decrease in Si content, respectively. Thus, it was confirmed that no specific element losses were observed after repeating the photothermal effect. The minimal decrease in element content was observed due to the higher temperature but not the bacteria–nanoparticle

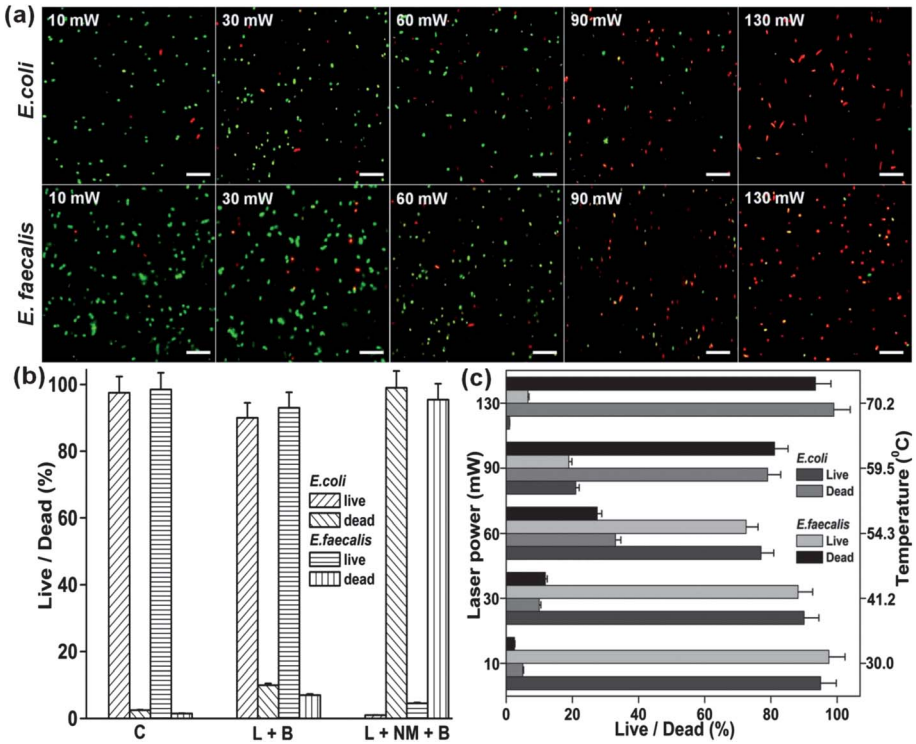

Fig. 3 (a) Fluorescence microscopy images of bacteria after exposure to the extending laser power from 10 mW to 130 mW, imaged at 100× magnification. Scale bar = 15 μm. (b) Quantitative bacteria cell lyses. Percentage survival of bacterial cells (counted with live/dead bacteria kit). C = control; L + B = laser irradiation on bacteria containing no nanoparticles; L + NM + B = laser irradiation on a mixture of nanoparticles and bacteria. (c) Graph shows the quantified survival rate of bacteria with increasing laser power and its corresponding temperature increase.

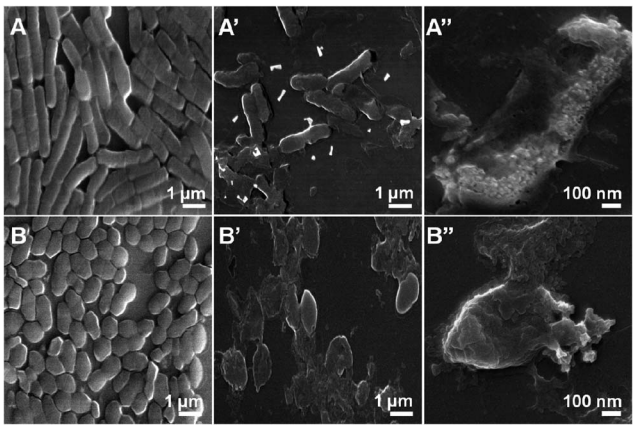

Fig. 4 (A) and (B) are SEM images of untreated cells of *E. coli* and *E. faecalis*. (A′) and (B′) are cell wall ruptured dead bacteria, after laser-nanoparticle exposure. (A″) and (B″) are magnified images of lysed bacteria.

interaction. Further, from the magnified images from FE-SEM, there was no evidence of nanoparticle availability either on the surface or in the cellular contents of the bacteria. And the surface EDX spectra of the bacteria (data not shown) also did not show any elements except Si. The existence of Si may be due to the supporting substrate on which the bacteria were fixed. Hence, we successfully achieved the complete recovery of the GNR–MNPs after repeated laser illuminations.

In addition to confirming the cell death with live/dead dye, we quantitatively analyzed the spectrophotometric differences made by live and dead bacteria. The fluorescence intensity difference was examined after exciting at 470 nm. The dye treated bacterial suspension emission response was recorded at 520 nm for live cells (green fluorescence) and at 630 nm for dead cells (red fluorescence). Fig. 5 shows a time correlation diagram comparing to the relative fluorescence intensity unit (RFU). The gradual decrease in RFU at 520 nm for both bacteria represents a reduction in live cells upon laser exposure. In contrast, increased RFU at 630 nm indicate a significant increase in cell death which is in good agreement with the temperature increase and laser exposure time. The large alterations in spectroscopic intensities between live and dead cells suggest that after exposure, thermal diffusion propagates heat into the surrounding media which causes irreparable damage to the bacteria cells.

The optical density measurement indicates the density of the bacteria in the medium. We used this parameter to represent the biocidal activity of the photo-thermally treated bacteria. The bacterial lysis profile (ESI, Fig. ES1a†) reveal that the OD_{600} started to decrease during the increasing temperature increments. The absorption dramatically dropped after the temperature rose to more than 50 °C. Thereafter the absorption decreased steadily and at 70 °C there was no absorption at OD_{600}. From these linear fit curves the maximum bactericidal temperature (MBT) was obtained for each bacterium separately.

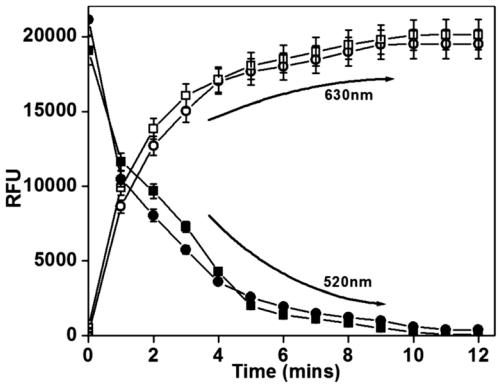

Fig. 5 Time based correlation of cell lysis spectrographs. (a) The solid and open squares represent the corresponding RFU of live and dead *E. coli*, respectively; the solid and open circles represent the corresponding RFU of live and dead *E. faecalis*, respectively.

These values were in good agreement with the RFU data (Fig. 5). The results demonstrated the excellent biocidal capability of GNR–MNPs after laser irradiation. The strong decrease in optical density values support the hypothesis of bactericidal activity *via* the photothermal effect with GNR–MNPs.

The thermal history of both the laser irradiated and hot-plate methods and their temperature increasing pattern with time were described (ESI, Fig. ES2†). Compared to room temperature, the laser irradiation produced a sudden photothermal effect resulted in a high temperature of approximately 60 °C in one minute. The hot-plate caused a slow temperature rise to about 30 °C in the same time. But the hot-plate induced more than 90 °C at 12 min. Basically, there was a possible sustained heat loss from the surface heat source during the experiment due to heat dissipation, leading to increase the time required for heating. Hence, autoclaving is recommended for perfect sterilization instead of simple open heat procedures. But autoclaving uses far more energy than hot-plates. Further this could not be controlled after attaining a required temperature while in continuous operation. More importantly, the laser light utilized only 130 mW to reach the higher temperature but the hot-plate system used approximately 850 W to achieve the maximum temperature. In addition, compared to our method, repeated use of the hot-plate method uses more time and energy.

For comparison to the photothermal effect on bacterial mortality the effect of direct heat from the heat bath was examined. In Fig. ES3(a) and (b), (see the ESI, Fig. ES3)† we show the images of heat treated bacteria samples at 40, 50, 60, 70, 80, 90 and 100 °C with reduced numbers of live *E. coli* and *E. faecalis*. Corresponding statistical results are presented in Fig. ES4 (see the ESI, Fig. ES4).† From the images it can be clearly seen that, a hot-plate heated bacteria suspension at 70 °C shows more than 50% bacteria survivial. In particular, more than 10% of the *E. faecalis* cells were viable at 100 °C while showing high pathogenicity. This is a considerably larger quantity as compared to our laser aided GNR–MNP method which shows >95% cell lysis rate. Compared to the hot-plate method our photothermal method resulted an immediate temperature rise and a superior bacteria lysis rate. Interestingly, in both the methods the Gram-negative *E. coli* showed a superior lysis rate as compared to Gram-positive *E. faecalis*. The kinetics of bacteria decomposition under heating depended on the nature of the outer cell membrane. Basically, Gram-positive bacteria exhibit more resistance towards heat than Gram-negative bacteria.[43] The heat produced from the hot-plate method resulted in a lower survival rate of *E. coli* than *E. faecalis*. In contrast, GNR–MNPs caused the photothermal effect resulting in higher killing rates of bacteria regardless of the cell wall composition. All together, our newly developed GNR–MNP, laser aided method achieved superior bactericidal activity of about 100% in a shorter period of time than the conventional, time consuming, energy intensive hot-plate method.

In comparison to conventional disinfection techniques, photothermal treatment with GNR–MNPs has several potential advantages which make them promising anti-bacterial agents. First, the MNP conjugated GNRs can be collected easily and reused several times without losing components. Second, the method allows precise control over the temperature range and distribution by changing the nanoparticle concentration, laser energy and irradiation time. Third, compared to conventional sterilization methods, especially, to slow heating methods this method provides a faster rate of bacteria destruction in buoyant systems. Finally, GNR–MNPs are biocompatible, reusable and highly effective against nosocomial pathogens. As an initial trial, we examined the photothermal effect with GNR–MNP. In order to apply this method in real time, we have to consider various parameters. Based on the results, we fabricated GNRs with MNPs and optimized the photoheating efficiency against two bacteria strains by controlling all parameters, including nanoparticle concentration, radiant energy and exposure time. In addition to evaluate the irradiation response of GNR–MNPs, other types of microorganisms at higher populations will also be analyzed to evaluate the temperature dependent bactericidal effect. Although this is an initial trial to control floating bacteria by photothermal techniques further optimized conditions can be used to apply GNR–MNPs to publicly accessible water purifier devices to improve societal health benefits by preventing the spread of bacteria related infections.

Conclusions

In conclusion, GNR–MNPs were synthesized by nucleophilic reaction between nanomaterials and characterized using electron microscopy. The anti-bacterial activities of GNR–MNPs toward Gram-negative and Gram-positive strains were studied. When the NIR irradiation correlates with the SPR of GNR a rapid increase in temperature is observed. This photothermal effect causes irreparable cellular destruction of the bacteria in a quick manner, as compared to slow hot-plate heating. Repeated laser irradiation on the same GNR–MNP after magnetic separation resulted in a similar temperature increase for more than three consecutive times without any loss of nanoparticles. The change in laser energy and nanoparticle concentration shows a direct impact on bacterial viability. The results of this study showed that the combined photothermal treatment using the GNR–MNPs and a NIR laser can be applied as a highly effective, rapid, direct,

repeatable, and real-time method for eradication of microbial contaminants. Therefore, we believe this approach may be used as a better strategy for providing water that is free from contamination by other types of microbes as well as viral agents.

Acknowledgements

This research was supported by Korean NRF, NRF-2013R1A1A2005329.

References

1 C. J. Murphy, T. K. Sau, A. M. Gole, C. J. Orendorff, J. Gao and L. Gao, *J. Phys. Chem. B*, 2005, **109**, 13857–13870.
2 D. K. Yi, I. C. Sun, J. H. Ryu, H. Koo, C. W. Park, I. C. Youn, K. Choi, I. C. Kwon, K. Kim and C. H. Ahn, *Bioconjugate Chem.*, 2010, **21**, 2173–2177.
3 L. Cognet, S. Berciaud, D. Lasne and B. Lounis, *Anal. Chem.*, 2008, **80**, 2289–2294.
4 C. Sönnichsen and A. P. Alivisatos, *Nano Lett.*, 2005, **5**, 301–304.
5 C. Yu and J. Irudayaraj, *Anal. Chem.*, 2007, **79**, 572–579.
6 C. J. Murphy, A. M. Gole, S. E. Hunyadi, J. W. Stone, P. N. Sisco, A. Alkilany, B. E. Kinard and P. Hankins, *Chem. Commun.*, 2008, 544–557.
7 T. Kawano, Y. Niidome, T. Mori, Y. Katayama and T. Niidome, *Bioconjugate Chem.*, 2009, **20**, 209–211.
8 C. C. Chen, Y. P. Lin, C. W. Wang, H. C. Tzeng, C. H. Wu, Y. C. Chen, C. P. Chen, L. C. Chen and Y. C. Wu, *J. Am. Chem. Soc.*, 2006, **128**, 3709–3715.
9 P. K. Jain, X. Huang, I. H. El-Sayed and M. A. El-Sayed, *Plasmonics*, 2007, **2**, 107–118.
10 X. Huang, P. K. Jain, I. H. El-Sayed and M. A. El-Sayed, *Lasers Med. Sci.*, 2007, **23**, 217–228.
11 M. A. El-Sayed, *Acc. Chem. Res.*, 2001, **34**, 257–264.
12 D. K. Yi, *Mater. Lett.*, 2011, **65**, 2319–2321.
13 L. Tong, Q. Wei, A. Wei and J. X. Cheng, *Photochem. Photobiol.*, 2009, **85**, 21–32.
14 R. R. Letfullin, C. Joenathan, T. F. George and V. P. Zharov, *Nanomedicine*, 2006, **1**, 473–480.
15 J. R. Morones, J. L. Elechiguerra, A. Camacho, K. Holt, J. B. Kouri, J. T. Ramírez and M. J. Yacaman, *Nanotechnology*, 2005, **16**, 2346–2353.
16 V. P. Zharov, K. E. Mercer, E. N. Galitovskaya and M. S. Smeltzer, *Biophys. J.*, 2006, **90**, 619–627.
17 M. Veerapandian and K. S. Yun, *Appl. Microbiol. Biotechnol.*, 2011, **90**, 1655–1667.
18 C. B. Kim, D. K. Yi, P. S. Kim, W. Lee and M. J. Kim, *J. Nanosci. Nanotechnol.*, 2009, **9**, 2841–2845.
19 W. Jo, K. Freedman, D. K. Yi, R. K. Bose, K. K. S. Lau, S. D. Soloman and M. J. Kim, *Biofabrication*, 2011, **3**, 015002.
20 W. Jo, J. H. Lee and M. J. Kim, *J. Nanopart. Res.*, 2012, **14**, 1–11.
21 J. Silhan, C. B. Corfitzen and H. J. Albrechtsen, *Water Sci. Technol.*, 2006, **54**, 49–56.
22 C. Wang and J. Irudayaraj, *Small*, 2010, **6**, 283–289.
23 U. Tamer, I. H. Boyac, E. Temur, A. Zengin, I. Dincer and Y. Elerman, *J. Nanopart. Res.*, 2011, **13**, 3167–3176.
24 A. Gole, J. W. Stone, W. R. Gemmill, H. C. zur Loye and C. J. Murphy, *Langmuir*, 2008, **24**, 6232–6237.
25 U. Tamer, Y. Gundogu, I. H. Boyaci and K. Pekmez, *J. Nanopart. Res.*, 2009, **12**, 1187–1196.
26 L. Wang, J. Bai, Y. Li and Y. Huang, *Angew. Chem., Int. Ed.*, 2008, **47**, 2439–2442.
27 S. Link and M. A. El-Sayed, *Int. Rev. Phys. Chem.*, 2000, **19**, 409–453.
28 B. Nikoobakht and M. A. El-Sayed, *Chem. Mater.*, 2003, **15**, 1957–1962.
29 T. K. Sau and C. J. Murphy, *Langmuir*, 2004, **20**, 6414–6420.
30 D. K. Yi, S. S. Lee, G. C. Papaefthymiou and Y. Jackie, *Chem. Mater.*, 2006, **18**, 614–619.
31 N. R. Jana, L. Gearheart and C. J. Murphy, *J. Phys. Chem. B*, 2001, **105**, 4065–4067.
32 A. Rosowsky, in *The Chemistry of Heterocyclic Compounds*, ed. A. Weissberger, Interscience Publishers, New York, 1964, vol. 19, 1, p. 1.
33 *Chemistry and Technology of Epoxy Resins*, ed. B. Ellis, Blackie Academic & Professional, Glasgow, 1993, pp. 117–143.
34 M. Hu, J. Chen, Z. Y. Li, L. Au, G. V. Hartland, X. Li and Y. Xia, *Chem. Soc. Rev.*, 2006, **35**, 1084–1094.
35 B. Hu, L. P. Zhang, X. W. Chen and J. H. Wang, *Nanoscale*, 2013, **5**, 246–252.
36 L. Tong, Q. Wei, A. Wei and J. X. Cheng, *Photochem. Photobiol.*, 2009, **85**, 21–32.
37 W. An, Q. Zhu, T. Zhu and N. Gao, *Exp. Therm. Fluid Sci.*, 2013, **44**, 409–418.
38 W. C. Huang, P. J. Tsai and Y. C. Chen, *Small*, 2009, **5**, 51–56.
39 D. K. Yi, *Mater. Lett.*, 2011, **65**, 2319–2321.
40 J. W. M. Chon, C. Bullen, P. Zijlstra and M. Gu, *Adv. Funct. Mater.*, 2007, **17**, 875–880.
41 C. Gautier, A. Cunningham, L. Si-Ahmed, G. Robert and T. Burgi, *Gold Bull.*, 2010, **43**, 94–104.
42 R. Zou, Q. Zhang, Q. Zhao, F. Peng, H. Wang, H. Yu and J. Yang, *Colloids Surf., A*, 2010, **372**, 177–181.
43 M. C. Wu, A. R. Deokar, J. H. Liao, P. Y. Shih and Y. C. Ling, *ACS Nano*, 2013, **7**, 1281–1290.
44 B. Hu, L. P. Zhang, X. W. Chen and J. H. Wang, *Nanoscale*, 2013, **5**, 246–252.
45 J. Borovička, W. J. Metheringham, L. A. Madden, C. D. Walton, S. D. Stoyanov and V. N. Paunov, *J. Am. Chem. Soc.*, 2013, **135**, 5282–5285.

